Title

Isolation and characterization of human embryonic stem cell-derived heart field-specific cardiomyocytes unravels new insights into their transcriptional and electrophysiological profiles

Journal

Cardiovascular Research, 118(3)

ISSN

1015-5007

Authors

Pezhouman, Arash
Engel, James L
Nguyen, Ngoc B
et al.

Publication Date

2022-02-21

DOI

10.1093/cvr/cvab102

Peer reviewed

ESC European Society of Cardiology

Cardiovascular Research (2022) **118**, 828–843
doi:10.1093/cvr/cvab102

Isolation and characterization of human embryonic stem cell-derived heart field-specific cardiomyocytes unravels new insights into their transcriptional and electrophysiological profiles

Arash Pezhouman [1,2†], James L. Engel [1,2†], Ngoc B. Nguyen[1,2,3†], Rhys J.P. Skelton[1,2], William Blake Gilmore [1,2], Rong Qiao[1,2], Debashis Sahoo[4], Peng Zhao[1], David A. Elliott[5,6], and Reza Ardehali [1,2,3,7*]

[1]Division of Cardiology, Department of Internal Medicine, David Geffen School of Medicine, University of California, Los Angeles, CA 90095, USA; [2]Eli and Edythe Broad Stem Cell Research Center, University of California, Los Angeles, CA 90095, USA; [3]Molecular, Cellular and Integrative Physiology Graduate Program, University of California, Los Angeles, CA 90095, USA; [4]Departments of Pediatrics and Computer Science and Engineering, University of California San Diego, La Jolla, CA 92093, USA; [5]Murdoch Children's Research Institute, The Royal Children's Hospital, Parkville, VIC 3052, Australia; [6]Department of Paediatrics, The University of Melbourne, Parkville, VIC 3052, Australia; and [7]Molecular Biology Institute, University of California, Los Angeles, CA 90095, USA

Received 11 May 2020; revised 21 October 2020; editorial decision 3 March 2021; accepted 18 March 2021; online publish-ahead-of-print 21 March 2021

Aims We prospectively isolate and characterize first and second heart field- and nodal-like cardiomyocytes using a double reporter line from human embryonic stem cells. Our double reporter line utilizes two important transcription factors in cardiac development, TBX5 and NKX2-5. TBX5 expression marks first heart field progenitors and cardiomyocytes while NKX2-5 is expressed in nearly all myocytes of the developing heart (excluding nodal cells). We address the shortcomings of prior work in the generation of heart field-specific cardiomyocytes from induced pluripotent stem cells and provide a comprehensive early developmental transcriptomic as well as electrophysiological analyses of these three populations.

Methods and results Transcriptional, immunocytochemical, and functional studies support the cellular identities of isolated populations based on the expression pattern of NKX2-5 and TBX5. Importantly, bulk and single-cell RNA sequencing analyses provide evidence of unique molecular signatures of isolated first and second heart field cardiomyocytes, as well as nodal-like cells. Extensive electrophysiological analyses reveal dominant atrial action potential phenotypes in first and second heart fields in alignment with our findings in single-cell RNA sequencing. Lastly, we identify two novel surface markers, POPDC2 and CORIN, that enable purification of cardiomyocytes and first heart field cardiomyocytes, respectively.

Conclusions We describe a high-yield approach for isolation and characterization of human embryonic stem cell-derived heart field-specific and nodal-like cardiomyocytes. Obtaining enriched populations of these different cardiomyocyte subtypes increases the resolution of gene expression profiling during early cardiogenesis, arrhythmia modelling, and drug screening. This paves the way for the development of effective stem cell therapy to treat diseases that affect specific regions of the heart- or chamber-specific congenital heart defects.

* Corresponding author. Tel: +310 825 0819; fax: +310 206 5777, E-mail: rardehali@mednet.ucla.edu
† The first three authors contributed equally to this article.

Graphical Abstract

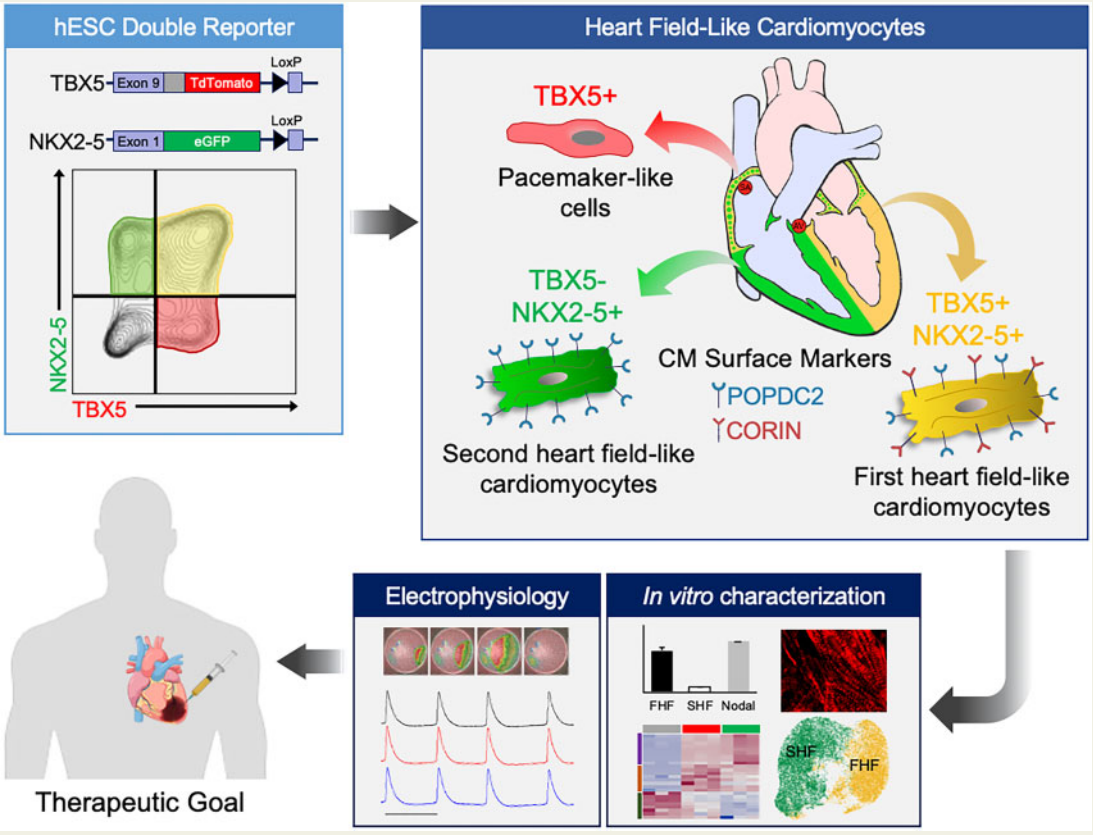

Keywords hESCs • Heart field-specific cardiomyocytes • Cardiac differentiation • Corin • Electrophysiology

1. Introduction

During early embryonic development, the primitive streak is derived from mesodermal cells under temporospatial effects of morphogens such as BMP4, Wnts, and Activin A. Mesodermal cells expressing Mesp1 migrate anteriorly and laterally to form the cardiac crescent and then the primitive heart tube.[1–5] This migratory group of cells includes two very distinct populations of cardiac progenitor cells (CPCs), namely the first and the second heart field (FHF and SHF, respectively).

The FHF is identified by expression of Hcn4 and Tbx5,[6,7] before giving rise to the left ventricle (LV) and part of the atria, whereas the SHF is marked by transient expression of Tbx1, Fgf8/10, Isl1, and Six2, and exclusively contributes to the outflow tract (OT), the right ventricle (RV), and part of the atria.[8–11] Cells from the SHF are highly proliferative and migratory and are primarily responsible for the elongation and looping of the heart tube. Additionally, SHF cells differentiate to cardiomyocytes (CMs), fibroblasts, smooth muscle, and endothelial cells as they enter the heart tube, while the FHF cells are less proliferative and mostly become CM.[6,12]

Attempts to identify heart field-specific CPCs have been made in rodent models marking cardiac cells that express ISL1 and TBX5. ISL1 becomes restricted to SHF during the elongation of the pre-heart tube before being downregulated,[11,13–15] establishing temporal expression of ISL1 as a viable marker of the SHF *in vivo*. However, ISL1 also marks cells from other lineages, including β-islet cells.[16] As such, cardiac directed human embryonic stem cell (hESC)-derived ISL1^{+} populations commonly consist of a mixture of CM subtypes and non-myocyte cells.[17] During early development, TBX5 was shown to be highly expressed in forelimbs, trachea, lung, heart, and the thoracic wall. Lower levels of TBX5 were found in the retina and telencephalon.[18] Investigators have shown that within the heart, *TBX5* is predominately expressed in the primitive posterior heart tube, marking progenitors of the LV and atria, corresponding to the FHF.[6,7,19–21] Further characterization showed that TBX5 expression is limited to the heart and limbs in later stages of development.[22] While these animal models have provided substantial information regarding *in vivo* cardiac lineage formation, there is a need to design an *in vitro* tool to not only investigate heart field specification but also enrich for chamber-specific CMs.

The *in vitro* differentiation of hESCs recapitulates many aspects of early human development and provides insight into an otherwise inaccessible period of embryogenesis. hESCs have been used to derive cardiac differentiation schemes based on signalling pathways that direct *in vivo* cardiogenesis.[23–25] These studies have been assisted by the generation of several cardiac reporter lines, which have been used to enrich for cardiac CPCs as well as their definitive progeny (atrial, ventricular, and nodal cells).[13,26,27] While some investigators have developed strategies to

isolate mature CMs using genetic markers such as troponin and myosin heavy chain, others have targeted early cardiac-related transcription factors such as MESP1 and NKX2-5, which are essential for cardiac cell fate specification.[28–32] The primary limitation of these strategies is the generation of a heterogeneous cell population, which confounds *in vitro* studies of CM lineage specification and may result in poor cell engraftment and potential arrhythmias post-transplantation.[33–35] The inability of the transplanted cells for structural integration and contamination with cell types that may serve as a nidus for arrhythmias are major safety concerns that need to be addressed prior to clinical application.[36] An ideal candidate for regenerative therapy for left ventricular myocardial infarction would be cells that most closely represent the ontogeny of the native tissue, namely left ventricular CMs. In order to generate this highly specialized and homogenous CM population, two key milestones must be achieved, which are (1) heart field specification (FHF/SHF) and (2) CM subtype (atrial/ventricular).

TBX5 has been shown to interact with NKX2-5, an important transcription factor in cardiac development.[37] Developmental studies have shown that *NKX2-5* is expressed in nearly all myocytes of the developing heart, excluding sinoatrial nodal-like pacemaker cells.[38] In a recent study, Zhang et al. developed a human induced pluripotent stem cells (hiPSCs) double reporter using TBX5 and NKX2-5 in which they reported isolation of FHF- and SHF-like CMs as well as endothelial and epicardial lineages (containing nodal-like cells).[39] While they went on to characterize these populations using various methodologies, they reported ISL1 expression in both their nodal-like population (arising from $TBX5^{+}$ cells) as well as their SHF-like population (arising from $TBX5^{-}$ cells), which raises the question that TBX5 may not be a specific marker to distinguish the cardiac heart fields *in vitro*. Possibilities attributing to this discrepancy with previous studies may be due to: (1) differences between rodents and humans, (2) ectopic and transient expression of ISL1 in different cardiac cell types during development, or (3) the use of terminally differentiated somatic cells that were reprogrammed into a pluripotent state may not be ideal for examining events that happen during early cardiogenesis *in vitro*.

To address the limitations above, we developed a double reporter (*TBX5-TdTomato*$^{+/W}$/*NKX2-5*$^{eGFP/W}$) using hESCs to determine whether FHF- and SHF-like CMs delineated by TBX5 show transcriptional profiles that mirror those reported in hiPSCs or are more similar to the previous *in vivo* models. Considering the previous reports of low efficiency for heart field-specific cardiac differentiation scheme in hiPSCs of about 20%, we optimized the differentiation protocol to consistently generate over 80% of FHF-like CMs. While our generated FHF- and SHF-like CMs shared some similarities with previously reported hiPSCs-derived CMs, we found differences in their transcriptional and functional profiles. We further identified potential surface markers (POPDC2 and CORIN) that can be used to isolate CMs and FHF-like CMs without the use of a genetically modified reporter line, making it more suitable for clinical application. These findings permit the efficient and reproducible differentiation strategies to generate FHF-, SHF-, and nodal-like CMs *in vitro*, which could be used for: 1) modelling diseases that specifically affect either the left or right regions of the heart, 2) investigating cardiac development and lineage specification *in vitro*, and 3) generating highly enriched populations of LV CMs to advance cellular-based regenerative therapies.

2. Methods

2.1 Generation of reporter cell lines

The hESC HES3-*NKX2-5*$^{eGFP/W}$ reporter cell line (passage 12) was generously provided by E. Stanley and A. Elefanty (Monash University, Victoria, AU) and was generated by targeting the eGFP coding sequence to the *NKX2-5* locus of HES3 cells using previously described protocol.[27] The HES3-*TBX5-TdTomato*$^{+/W}$/*NKX2-5*$^{eGFP/W}$ double reporter line was generated using TALEN technology. A T2A self-cleaving peptide followed by TdTomato gene was incorporated in-frame into the last exon (Exon 9) of *TBX5* without affecting its 3'UTR. The *TBX5-T2A-TdTomato* donor vector was built to contain left and right homology arms (800 bp–1000bp) that flank the genomic cleavage site in the *TBX5* locus. PCR of the 5' junction of the integrated TdTomato construct directly downstream and in-frame with the endogenous Tbx5 gene was performed using the following primers: forward: 5′-TGCACAACTGCACCTGGTTAGTTG and reverse: 5′-TCTTCACCTTGTAGATCAGCGTGC. Karyotyping was performed using the KaryoStat service (ThermoFisher). Cells from passages 20–40 of the double reporter were used for this study.

2.2 Teratoma formation assay for assessment of cell line pluripotency

Animal studies were performed according to the guidelines of UCLA's Animal Care And Use Committee (IACUC) and the National Institutes of Health (NIH) Guide for the Care and Use of Laboratory Animals. All animal protocols in this study were reviewed and approved by Chancellor's Animal Research Committee (ARC). Adult male NSG mice (8–10 weeks old) were intubated and anaesthetised with isoflurane (3–5%). After a transverse incision to expose the kidney, $5x10^5$ cells resuspended in growth factor reduced Matrigel and RPMI B27 (1:1) were injected directly underneath the capsular membrane of the kidney using a 26-gauge Hamilton syringe. The kidney was then gently repositioned into the abdominal cavity, and the muscle and skin were sutured. Postoperatively, animals were received oxygen, pain medications (buprenorphine twice daily), and close monitoring for any signs of distress. Four weeks after transplantation, the mice were euthanized by 10-min isoflurane inhalation (15–30%) followed by cervical dislocation, and teratoma tissues were rapidly collected and fixed in 4% paraformaldehyde.

2.3 Differentiation of hESC

Monolayer differentiations of CMs were carried out using the GiWi strategy as previously described.[40] Briefly, HES3-*TBX5-TdTomato*$^{+/W}$/*NKX2-5*$^{eGFP/W}$ or H9 (WiCell) hESCs were grown on Geltrex (Gibco™, A1413202) to 90% confluency then harvested as single cell suspension using Accutase (Gibco™, A1110501)) and resuspended in mTeSR1 (Stem Cell™ Technologies, 85852) containing 10 μM ROCK inhibitor Y-27632 (Tocris Biosciences, 1254). Cells were counted using a Countess II Automated Cell Counter (Countess™, AMQAX1000) and re-plated onto Geltrex coated plates at 1.3×10^5 cells/cm^2 for FHF ($TBX5^{+}NKX2\text{-}5^{+}$), 2.0×10^5 cells/cm^2 for SHF ($TBX5^{-}NKX2\text{-}5^{+}$) and 3.0×10^5 cells/cm^2 for nodal ($TBX5^{+}NKX2\text{-}5^{-}SIRP\alpha^{+}CD90^{-}$) in mTeSR1 containing 10 μM ROCK inhibitor Y-27632 (Day 2 of differentiation). At Day 1, media was changed to mTeSR1. At Day 0, media was changed to RPMI (Gibco™, 11875093) containing B-27™ supplement, minus Insulin (Gibco™, A1895601) containing CHIR99021 (Tocris, 4423) (10 μM for FHF, 6 μM for SHF and 12 μM for nodal). After 24 hr

(Day 1), media was changed to RPMI B27-ins until Day 3. On Day 3 of differentiation, cells were changed to RPMI B27-ins containing 5 μM IWP2 (Tocris, 3533). At Day 5, media was changed to RPMI B27-ins until Day 7 when media was switched to RPMI containing B-27™ supplement (Gibco™, A3582801). Cells were maintained in this media and changed every 3 days thereafter.

2.4 Flow cytometry and cell sorting

Differentiated hESCs were dissociated with TrypLE Express (Gibco™, 12604021) for 3–4 min at 37°C to form a single-cell suspension. Antibody labelling of cells was performed using anti-SIRPα PE-Cy7 (Biolegend, 323807), anti-Tra1-60 (Abcam, ab16288), anti-CD90 APC (Biolegend, 328113), anti-Podoplanin PE-cy7 (Biolegend, 337013), anti-CORIN (KAN Research Institute Inc.), anti-TNNT2 BV421 (BD Biosciences, 565618), and anti-mouse IgG APC (Biolegend, 405308). All antibodies were used at a dilution of 1:100. All antibodies were diluted and incubated in FACS buffer (2% FBS, 1% BSA, 2 mM EDTA) containing 10 μM ROCK inhibitor Y-27632. Samples were incubated with antibodies for 30–60 min on ice and washed using FACS buffer. Control stains using non-specific antibodies (IgG) were performed. Cells were sorted using a FACS-ARIA (BD Biosciences) into RPMI B27 with 10 μM ROCK inhibitor Y-27632. Flow analysis was performed using a Fortessa flow cytometer (BD Biosciences) and analysed using FlowJo software (Tree Star Inc.). For intracellular staining of TNNT2, cells were first stained for CORIN as described above, washed and incubated with anti-mouse IgG APC secondary for 30 min on ice in FACS Buffer, then stained for TNNT2 using the BD Cytofix/Cytoperm fixation and permeabilization kit (BD Biosciences) according to the manufacturer's instructions.

2.5 Bulk RNA sequencing

Total RNA of the cells was isolated using TRIZOL LS Reagent (Invitrogen™, 10296028), chloroform extraction, and isopropanol precipitation followed by further purification using RNeasy Micro kit (Qiagen, 74004). The quality of the RNA was assessed by Agilent 2200 Tapestation. For library preparation, total RNA was fragmented and subjected to cDNA conversion, adapter ligation, and amplification using KAPA Stranded RNA-Seq Library Preparation Kit (KAPA Biosystems, KK8502) according to the manufacturer's instructions. The final library was quantified using Agilent 2100 Bioanalyzer to evaluate its integrity. The deep sequencing for 2x150 bp paired-end reads was performed using Illumina Novaseq 6000. For sample analysis, RNA-seq data were mapped to the reference genome (GRCh38) with OLego version 1.1.5[41] and normalized by using TPM (Transcripts per millions) analysis. Total number of reads mapped to a known transcript annotation was estimated using featureCounts version v1.5.0-p2.[42] Expression levels for each transcript were determined by normalizing the counts returned by featureCounts using custom Perl scripts. Normalized expression levels for each transcript were determined by transforming the raw expression counts to TPM following log2 scaling. Gene ontology (GO) enrichments were computed using DAVID Bioinformatics Resources v6.7. Surface marker analysis was performed using PANTHER Classification System. RStudio was used to run custom R scripts to generate boxplots and heatmaps using 'heatmaply' package.

2.6 Patch clamp

For electrophysiological (EP) characterization using patch-clamp, cultured cells were dissociated and respective cell populations were isolated by FACS as described above. Isolated cells were resuspended in RPMI B27 supplemented with 10 μM ROCK inhibitor Y-27632 at 1-2x10^6 cells/ml. Drops of 25 μl of this cell suspension were applied to glass cover slips (5 mm) that were pre-coated with Geltrex in 6-well plates. The cells were incubated in the 25 μl volume for 8–12 hr to facilitate cell attachment. The dishes were then flooded with 2 ml of RPMI B27 supplemented with 10 μM ROCK inhibitor Y-27632. ROCK inhibitor was removed after 24 h, and the media was changed every 2 days. Cultures were used for patch clamp recordings 4–14 days following plating. Action potentials were measured using standard patch-clamp techniques in current-clamp modes (Axopatch 200B, Axon Instruments). Voltages were recorded with 2 KHz sampling rate (DigiData 1200, Axon Instruments) and analysed with Clampfit software (Axon Instruments). Borosilicate glass microelectrodes were used with tip resistances of 2–5 MΩ when filled with pipette solution.

2.7 Monolayer optical mapping

For high-resolution optical mapping of action potential (AP) propagation, cultured cells were dissociated and respective cell populations were isolated by FACS as described above. Isolated cells were suspended in RPMI B27 supplemented with ROCK inhibitor Y-27632 (10 μM) at 20–22x10^6 cells/ml. Drops of 25 μl of this cell suspension were applied to Geltrex-coated 5 mm coverslips (5x10^5 cells/coverslip). The cells were incubated in the 25 μl volume for 8-12 hr to facilitate cell attachment. Once spontaneous contractions were observed, cells were stained with voltage-sensitive dye, Di-8-ANEPPS (Invitrogen, D3167, 40 μM;) and washed with normal Tyrode solution three times. Optical AP recording were made using MiCAM-Ultima CMOS camera at 500 frames per second (fps). First, spontaneously occurring APs were recorded, followed by overdrive electrical pacing (1 Hz, 0.5 Hz). The basic cycle length was gradually decreased until loss of 1:1 capture or re-entry was induced. For APA measurements of only atrial cells, the surface of the optical mapping was divided into three partitions and 26 pixels with atrial morphology (triangulation) were selected from each partition.

2.8 Chronotropic response to β-adrenergic agonist and antagonist

Day 10 FACS isolated cells were re-plated on Geltrex coated dishes for 7–10 days. Basal beating rates were counted using a light microscope then 1 μM Isoprenaline hydrochloride (Sigma, I5627) was added and incubated at 37°C for 5 min before beating rates were counted again. 10 μM Propranolol hydrochloride (Sigma, P0884) was then added, incubated at 37°C for 5 min, and beating rate counted again.

2.9 Statistics

All data are represented as individual values. Due to the nature of the experiments, randomization was not performed and the investigators were not blinded. Statistical significance was determined by using Student's *t*-test (unpaired, two-tailed) or one-way ANOVA in GraphPad Prism 8 software. Results were significant at $P < 0.05$ (*), $P < 0.01$ (**), $P < 0.001$ (***), and $P < 0.0001$ (****). All statistical parameters are reported in the respective figures and figure legends. All error bars are depicted as SEM.

2.10 Study approval

The collection and use of human foetal material were carried out following federal and local approval, including the USA Institutional Review Board (IRB 11-002504) to the Translational Pathology Core Laboratory of the Department of Pathology and Laboratory Medicine at UCLA.

Cardiac tissues from human embryos were collected with written informed consent following surgical termination of pregnancy and staged immediately by stereomicroscopy according to the Carnegie classification. All identifiers were removed before obtaining the samples. This study is in compliance with the Declaration of Helsinki as demonstrated by our local IRB review and approval.

3. Results

3.1 Generation of a heart field-specific hESC reporter line

To generate a double reporter line for isolation of heart field-specific CMs from hESCs, we introduced the *TdTomato* (*TdT*) gene into the *TBX5* locus of a previously characterized HES3-*NKX2-5*$^{eGFP/W}$ hESC line by TALEN-mediated homologous recombination.[27] To avoid *TBX5* haploinsufficiency, the TALEN targeting strategy was designed such that the *TdT* sequences were fused with exon 9 (last exon) of *TBX5* via a linker encoding the T2A peptide, which allowed accurate reporter expression while maintaining biallelic expression of TBX5 (Supplementary material online, *Figure S1A*). This is an improved methodology to the previous report where a fluorescent gene was inserted in exon 1 which may lead to the compromised physiological function of TBX5.[39] The correctly targeted clone was identified by PCR analysis using specific TBX5 primers (Supplementary material online, *Figure S1B*) and karyotyping confirmed the absence of chromosomal abnormalities (Supplementary material online, *Figure S1C*). This *TBX5*$^{TdTomato+/W}$/*NKX2-5*$^{eGFP/W}$ hESC line expressed pluripotency markers, including *SOX2*, NANOG, OCT3, TRA1-60 after several passages (Supplementary material online, *Figure S1D*). Transplantation of this undifferentiated hESC line under the kidney capsule exhibited successful differentiation into teratomas contributing to all three germ layers (Supplementary material online, *Figure S1E*).

We first explored the lineage commitment of TBX5-marked cells using a monolayer cardiac differentiation protocol (*Figure 1A*).[40] Flow cytometry and fluorescent imaging on Days 0, 7, and 10 of differentiation show a progressive increase in the expression of TdT (*Figure 1B*). We performed immunocytochemistry (ICC) for cardiac structural protein TNNT2 and cardiac transcription marker TBX5 on differentiated Day 10 cells (*Figure 1C* top) to confirm their differentiation towards a CM fate, and ACTN2 and TNNT2 on differentiated Day 60 cells, which provide insights that they can efficiently differentiate into mature CMs (*Figure 1C*, bottom).

3.2 Transcriptional profiling of TBX5$^+$ and TBX5$^-$ populations reveals distinct heart field-like molecular signatures

To determine whether expression of TBX5 can distinguish FHF from SHF identity, we performed bulk RNA sequencing of undifferentiated hESCs (Day 0) and FACS-isolated TBX5$^+$ and TBX5$^-$ populations (Day 7) (*Figure 1D and E*). As expected, transcriptional analysis confirms reduced expression of pluripotency markers in the differentiated cells compared to hESCs. Genes related to cardiac contraction such as *TNNT2, MYH6,* and *ACTN2* are expressed in both TBX5$^+$ and TBX5$^-$ populations on Day 7, although there is relatively higher expression of many contractile genes within TBX5$^+$ cells. Genes related to endothelial, fibroblast, and smooth muscle are detected in both populations. While expression of endothelial and fibroblast genes is higher in TBX5$^-$ population, we observe greater expression of genes related to smooth muscle cells in TBX5$^+$ population. Interestingly, we observe enrichment of SHF markers (*ISL1, FOXA2, BMP4*) in TBX5$^-$ populations. The concomitant expression of cardiac contractile genes and *ISL1* hints towards the possibility that TBX5$^-$ progenitors may consist of SHF-like CMs. Notably, nodal markers (*KCNJ3, HCN4, TBX18*) are highly enriched in TBX5+ population, suggesting that TBX5+ progenitors may consist of FHF- and nodal-like cells. To determine whether the TBX5$^-$ population consists of CMs, we performed flow cytometry analysis to quantify the expression of intracellular TNNT2 between the TBX5$^+$ and TBX5$^-$ populations at Day 7. As shown in *Figure 1F*, 53.7% and 8.09% of cells are TNNT2$^+$ within TBX5$^+$ and TBX5$^-$ populations, respectively. Additionally, to confirm the flow cytometry results, sorted TBX5$^+$ and TBX5$^-$ cells were replated and ICC shows positive staining for TNNT2 and ACTN2 in both populations, albeit higher within the TBX5$^+$ population (*Figure 1G*).

3.3 Co-expression of NKX2-5 with TBX5 effectively enriches heart field-specific cardiomyocytes

Our transcriptional and molecular analyses revealed the presence of CMs within these two populations although to a lesser extent within TBX5$^-$ cells. Given these findings, we FACS isolated TBX5$^+$ and TBX5$^-$ cells that co-expressed NKX2-5 at Day 10 of cardiac differentiation for RNA sequencing to determine whether isolated TBX5$^+$/NKX2-5$^+$ and TBX5$^-$/NKX2-5$^+$ populations are further enriched for cardiac contraction genes while maintaining their commitment to heart field specificity (*Figure 2A*).

For RNA sequencing analysis, we compared Day 10 populations with our previous Day 7 TBX5$^+$ and TBX5$^-$ samples. Co-expression of NKX2-5 in TBX5$^-$ and TBX5$^+$ populations show higher expression of cardiac contraction related genes compared to isolated populations using TBX5 alone. Notably, expression of SHF markers such as *ISL1* and *TBX1* are significantly enriched in TBX5$^-$ and TBX5$^-$/NKX2-5$^+$ populations, providing further support that these CMs maintain their commitment to SHF specification (*Figure 2B*). Furthermore, GO analysis confirm that expression of NKX2-5 in TBX5$^-$ population helps to enrich for more cardiac-related pathways such as cardiac muscle cell development and energy production, consistent with our hypothesis that TBX5$^-$ populations contain cardiac cells that resemble SHF CMs at the transcriptional level (*Figure 2C*). As, on Day 7, TBX5$^+$ cells were enriched for cardiac related pathways, the addition of NKX2-5 enhanced cardiac-related pathways but not to the same extent as TBX5$^-$ populations (*Figure 2D*).

3.4 Tbx5/NKX2-5 double reporter enables isolation of heart field-specific cardiomyocytes and nodal cells

Recent investigations have reported the generation of nodal-like cells from hESC-derived CMs that do not express NKX2-5.[38] More recently, Zhang et al. isolated a population of epicardial cells that included nodal cells (defined as TBX5$^+$/NKX2-5$^-$) using their hiPSC double reporter.[39] However, ISL1, a well-established SHF marker, was found to be highly expressed in this population (Supplementary material online, *Figure S2A*). This finding raises the question whether nodal cells arise from FHF, SHF, or both. The unbiased differentiation of our hESC double reporter line also generated a distinct population of TBX5$^+$NKX2-5$^-$ cells (*Figure 2A*). In order to accurately characterize FHF-, SHF-, and nodal-like cells from our double reporter, we sought to optimize the cardiac differentiation protocols to achieve robust efficiency of each population, which enables more representative transcriptional analysis.

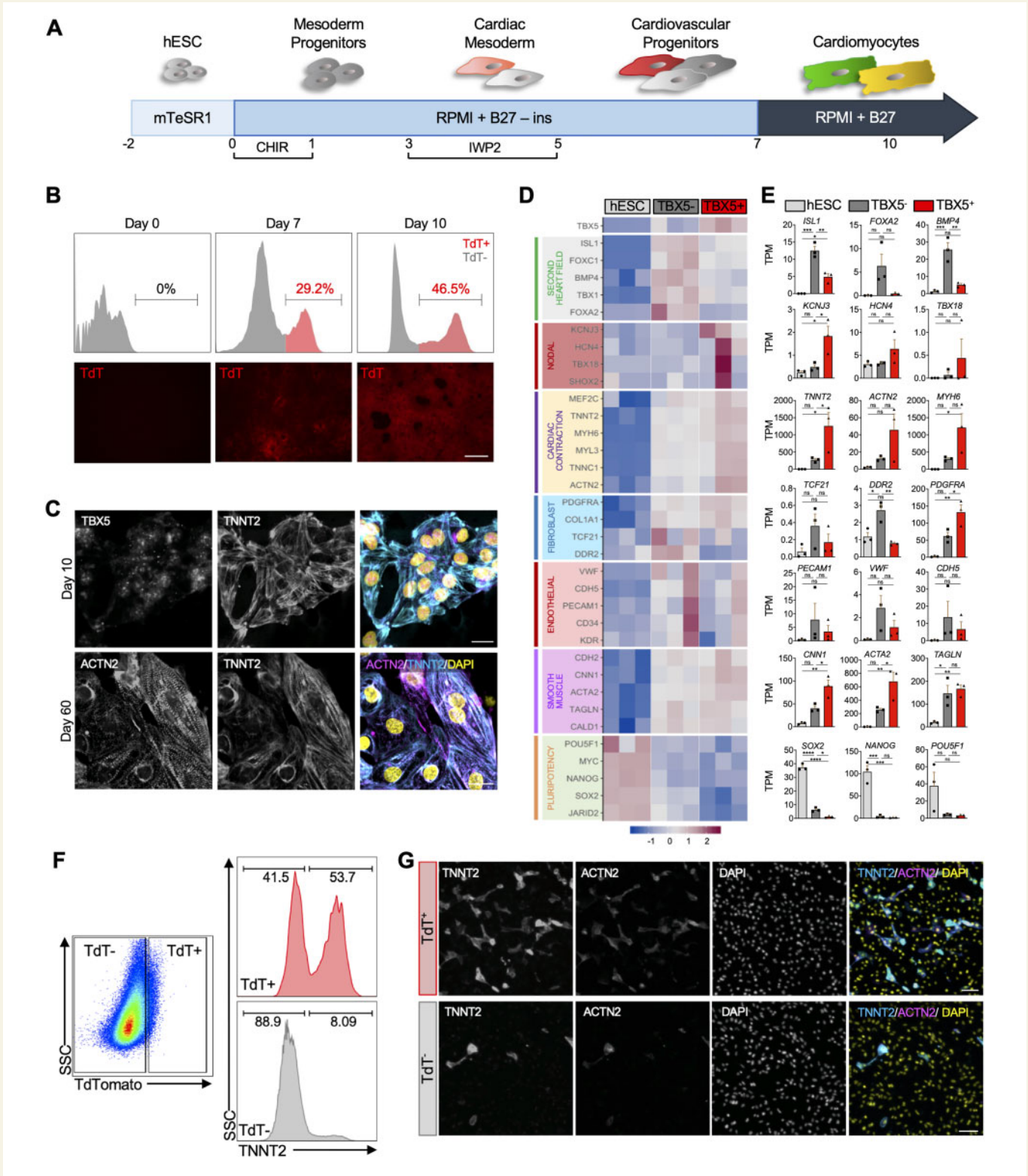

Figure 1 Generation and transcriptional profiling of heart field specific progenitors. (*A*) Schematic representation of the cardiomyocyte differentiation strategy used. (*B*) Flow cytometric analysis and fluorescent imaging of TdTomato (TdT) expression in differentiating hESCs at Days 0, 7, and 10. Scale bar = 200 μm. (*C*) Immunocytochemistry for cardiac progenitor TBX5, cardiac markers TNNT2 and ACTN2 on Days 10 and 60 of differentiation. Scale bar = 20 μm. (*D*) Heatmap and (*E*) bar plot of select genes from cardiac contraction, second heart field, pluripotency, and cell type specific gene groups in undifferentiated Day 0 hESCs and Day 7 $TBX5^+$ and $TBX5^-$ cells ($n = 3$ biological replicates per group), TPM = transcripts per million. (*F*) Flow analysis of intracellular $TNNT2^+$ within $TBX5^+$ or $TBX5^-$ populations. (*G*) Immunocytochemistry of TNNT2 and ACTN2 in sorted $TBX5^+$ and $TBX5^-$ cells. Scale bar = 100 μm. Statistical analysis is performed by using one-way ANOVA, $^*P < 0.05$, $^{**}P < 0.01$, $^{***}P < 0.001$, $^{****}P < 0.0001$, ns = not significant. Error bars = SEM.

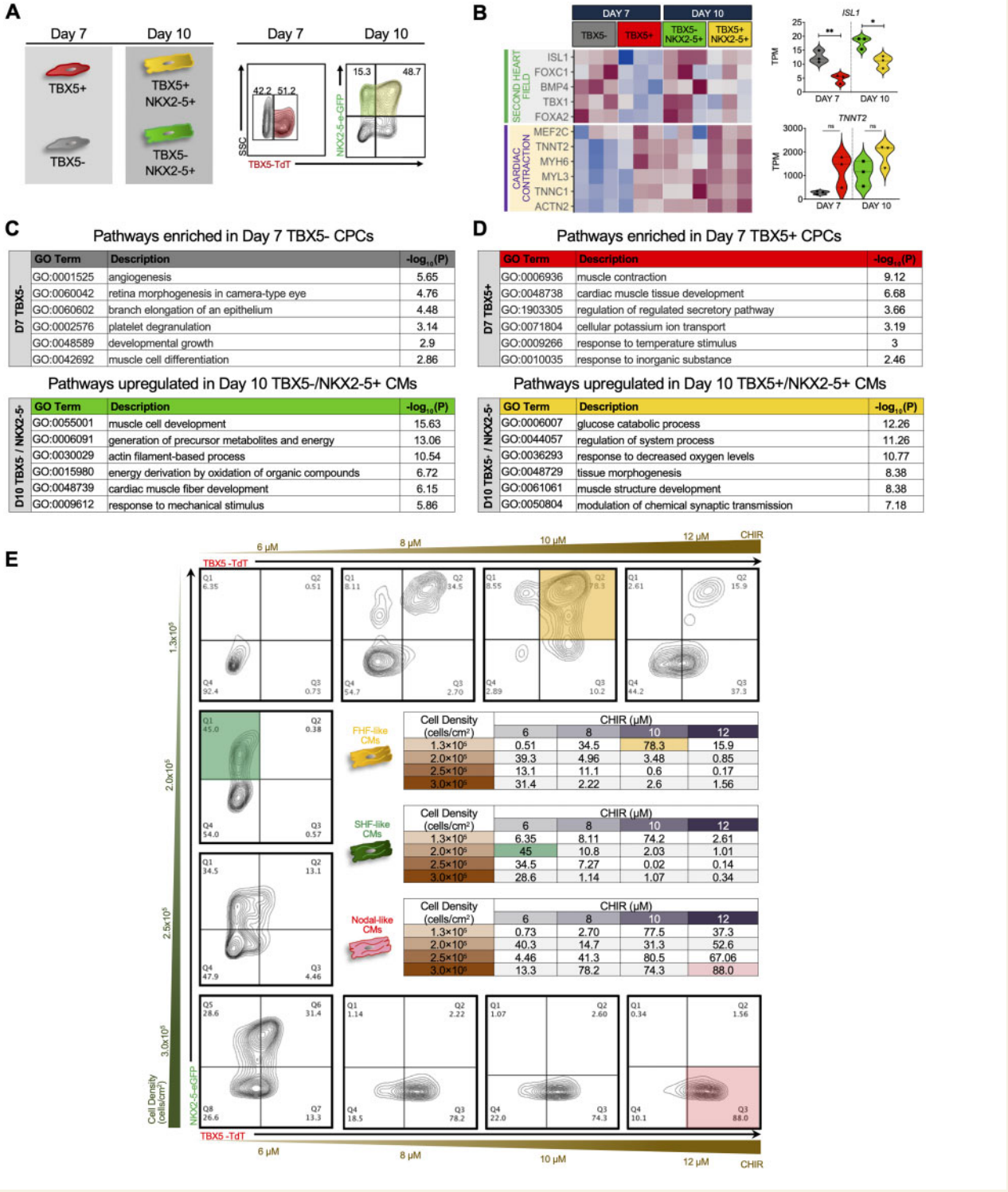

Figure 2 Transcriptional profiling of FHF- and SHF-like CMs at different cardiac differentiation stages. (*A*) Schematics and flow cytometric plots showing the cell sorting strategy for TBX5$^+$ and TBX5$^-$ populations at Days 7 (CPCs) and 10 (CMs) of differentiation. (*B*) Heatmap comparing cardiac contraction and second heart field related genes in TBX5$^+$ and TBX5$^-$ CPCs (Day 7) and CMs (Day 10). Violin plots of TNNT2 and ISL1 (right) of Days 7 and 10 populations ($n = 3$ biological replicates per group, Student's *t*-test, * $P < 0.05$, ** $P < 0.01$, TPM = transcripts per million). (*C*) GO analysis of pathways enriched in Day 7 TBX5$^-$ CPCs (top) and Day 10 TBX5$^-$ NKX2-5$^+$ CMs (bottom). (*D*) GO analysis of pathways enriched in Day 7 TBX5$^+$ CPCs (top) and Day 10 TBX5$^+$ NKX2-5$^+$ CMs (bottom). (*E*) Optimization of FHF and SHF cardiomyocyte populations via small-molecule modulation of Wnt signalling and cell seeding densities. Representative flow cytometric analysis at Day 10 of cardiac differentiation showing the expression of TBX5 and NKX2-5. Column represents varying seeding densities and row shows varying concentrations of CHIR99021 (CHIR). Inset tables show results from all combinations of seeding densities and CHIR concentrations. Yellow, green, and red highlighted boxes represent the maximum percentage of TBX5$^+$NKX2-5$^+$, TBX5$^-$NKX2-5$^+$, and TBX5$^+$NKX2-5$^-$ cells obtained, respectively (pool of three biological replicates).

We determined that out of all the variables involved in the cardiac differentiation process, seeding density and the concentration of the GSK-3β inhibitor (CHIR99021) had the most effect on directing the cardiac differentiation towards specific lineage commitment. Day 10 flow cytometry analysis reveals that plating densities of $1.3x10^5$ cells/cm^2 with 10 μM CHIR99021 or $2.0x10^5$ cells/cm^2 with 6 μM CHIR99021 provide the optimal conditions for the generation of TBX5$^+$NKX2-5$^+$ (FHF, 76.7 ± 1.3%) and TBX5$^-$NKX2-5$^+$ cells (SHF, 41.5 ± 1.8%), respectively. Additionally, a seeding density of $3.0x10^5$ cells/cm^2 with 12 μM CHIR99021 consistently results in greater than 80% TBX5$^+$NKX2-5$^-$ (nodal) cells with little contamination from other CM subtypes (*Figure 2E*, coloured boxes, Supplementary material online, *Figure S2B, Videos S1 and S2*).

For deeper transcriptional and molecular characterization, we FACS-isolated these three populations at Day 10 from separate customized differentiation cultures (*Figure 3A–C*). qPCR analysis of TBX5$^+$NKX2-5$^+$ cells show enrichment of FHF markers (*TBX5* and *HAND1*, (*Figure 3D*, left)) and lower expression of SHF markers (*ISL1* and TBX1, (*Figure 3E*, left)). Conversely, the TBX5$^-$NKX2-5$^+$ cells show increased expression of SHF markers and lower expression of FHF genes (*Figure 3D and E* left, and Supplementary material online, *Figure S2C*). Both populations express NKX2-5 as expected (*Figure 3F*). The lineage specificity of the hESC-derived FHF- and SHF-CMs is validated by their respective gene expression patterns, which closely mirror that of human foetal LV and right ventricle (RV) samples (gestation age 18 weeks) (*Figure 3D and E*, right and Supplementary material online, *Figure S2C*). Interestingly, we observe low expression level of ISL1 in populations in which TBX5 is high (i.e. FHF and nodal). This hints to the possibility that TBX5 may serve as a specific delineator of the heart fields.

Analysis of nodal-related genes *HCN4, TBX18,* and *SHOX2* reveals high levels within the TBX5$^+$NKX2-5$^-$ population in comparison to low or almost absent expression in FHF and SHF populations (*Figure 3F*). This further substantiates the ability of this reporter line to isolate FHF and SHF that excludes most nodal cells. Day 20 flow cytometry analysis show that approximately 60% of the TBX5$^+$NKX2-5$^-$ population is SIRPα$^+$CD90$^-$, consistent with a nodal-like phenotype (Supplementary material online, *Figure S2D*). Additionally, the majority of these cells (92%) also express Podoplanin, a marker for cardiac pacemaker cells (Supplementary material online, *Figure S2E*).[43] ICC analysis of TBX5$^+$NKX2-5$^+$, TBX5$^-$NKX2-5$^+$, and TBX5$^+$NKX2-5$^-$ isolated cells support gene expression results and confirm their CM phenotype with positive co-staining of TNNT2 with FHF (TBX5), SHF (ISL1), or nodal (SHOX2) markers (*Figure 3G–I*).

To examine whether prolonged culture affects the phenotype of these cells, Day 10 sorted cells were kept in culture for another 10 days (until Day 20 of differentiation). Transcriptional analysis of FHF and SHF on Day 20 shows the maintenance of heart field specificity during the maturation process as shown by higher expression of SHF markers in TBX5$^-$ compared to TBX5+ CMs. As expected, expression of pluripotency genes progressively decreases over time. We observe a decrease in the expression of cardiac contraction-related genes in both FHF and SHF CMs on Day 20 compared to Day 10 (Supplementary material online, *Figure S3A and B*). However, ICC analysis shows more organized and aligned sarcomeres in Day 20 FHF and SHF populations than Day 10, which reflects their phenotypic maturation at this later timepoint (Supplementary material online, *Figure S3C*).

Taken together, these data combined with the expression profiles observed in human foetal heart are in agreement with previous studies and demonstrate that the hESC *TBX5-TdTomato*$^{+/W}$*/NKX2-5*$^{eGFP/W}$ double reporter enables the prospective isolation and enrichment of heart field-specific CMs and nodal-like CMs from differentiating hESCs.

3.5 Transcriptomic analyses reveal enrichment of atrial-related genes in FHF- and SHF-like cardiomyocytes

In order to evaluate the molecular signatures, homogeneity, and chamber specificity of FHF- and SHF-like CMs, we performed single-cell RNA sequencing (scRNA seq) on both populations at Day 20 of cardiac differentiation (*Figure 4A*). We analysed a total of 9,699 FHF-like CMs and 11,815 SHF-like CMs. Dimensional reduction analysis reveals two distinct populations of cells corresponding to FHF- and SHF-like CMs, each comprising a single lobe in the uniform manifold approximation and projection (UMAP) distribution (*Figure 4B*). To confirm the CM identity of the isolated cells, we analysed the expression of the cardiac contraction genes, including *TNNT2, ACTN2,* and *MYH6* across our single cells. Although these genes are highly enriched in both populations, we observe higher expression levels in FHF-like CMs (*Figure 4C*). To examine whether these cells preferentially adopt an atrial or ventricular phenotype, we assessed the expression level of atrial and ventricular genes in these two populations. Both FHF- and SHF-like CMs express atrial-related genes (*MYL7, DKK3, NPPA*), with higher levels in FHF population (*Figure 4D*). On the other hand, there is low expression of ventricular markers (*MYL2, FHL2, IRX4*) in both populations, more noticeably in FHF-like CMs (*Figure 4E*). To evaluate potential contamination of FHF- and SHF-like CM populations with nodal cells, we analysed several nodal-related genes, such as *SHOX2, TBX18,* and *KCNJ3* which show absent or very low expression in the vast majority of CMs (*Figure 4F*). These results are confirmed by independent bulk RNA sequencing analysis which show similar trends in gene expression profiles (*Figure 4G*).

3.6 FHF- and SHF-like cardiomyocytes form functionally coupled monolayers and exhibit appropriate pharmacological responses

The myocardium forms a functional syncytium with individual CMs tightly coupled with adhesion junctions and connexins to provide mechanical and electrical connections. We sought to determine whether a 2-dimensional culture of FHF- and SHF-like CMs exhibit electromechanical connectivity by performing optical mapping.[44,45] Day 10 FHF- and SHF-like CMs were isolated and re-plated to form monolayers. Optical mapping signal analysis demonstrate spontaneous AP which exhibit almost similar contraction rates in FHF and SHF populations. Optical and isochronal activation maps of FHF-like CMs show uniform AP propagation throughout the monolayer with no block or changes in conduction velocity (CV= 0.11 m/s) (*Figure 5A* and Supplementary material online, *Figure S4A and Video S3*).[46] In SHF-like CM cultures, AP propagations were recorded from islands of cells (*Figure 5B* and Supplementary material online, *Video S4*) in which APs propagate independently, but uniformly, in each island. Although the spontaneous activity and the relatively rapid conduction in both FHF and SHF suggest the presence of a high-density inward current via voltage-activated channels, AP parameters are notably different between the two groups. Analysis of almost 10,000 APs reveal that the majority of APs from SHF population repolarize earlier and faster, resulting in shorter AP duration at 50% and 90% repolarization (APD_{50} and APD_{90}, respectively) compared to FHF-like CMs which show significantly longer APD_{50}, APD_{90}, and cycle lengths

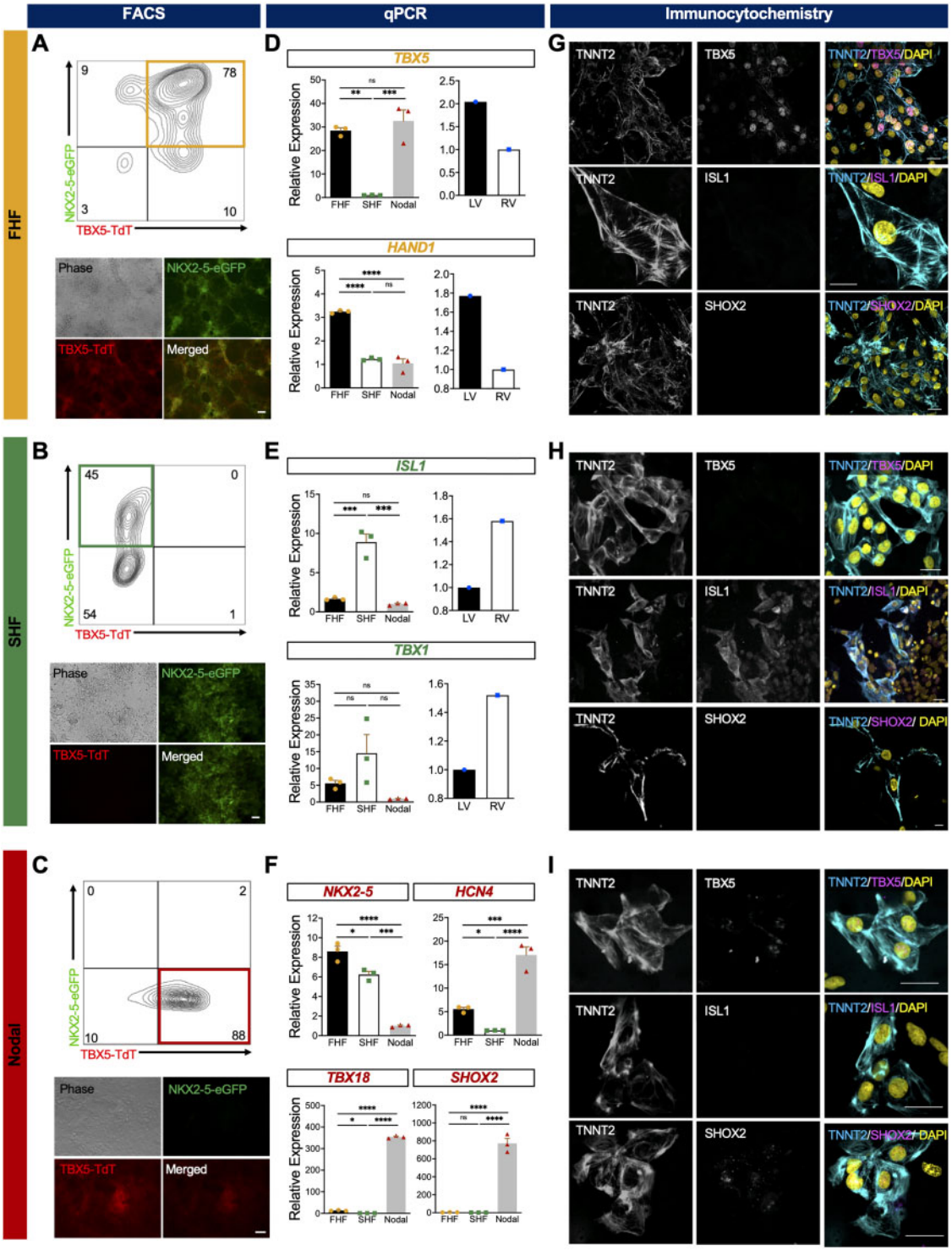

Figure 3 Characterization of hESC-derived FHF-, SHF-, and nodal-like cardiomyocytes. Fluorescence microscopy and representative flow cytometry plot of (*A*) TBX5^{+}NKX2-5^{+} (FHF), (*B*) TBX5^{-} NKX2-5^{+} (SHF), and (*C*) TBX5^{+}NKX2-5^{-} (nodal) optimized differentiations at Day 10 (pool of three biological replicates). Scale bar = 100 µm. Quantitative expression analysis of Day 10 sorted (*D*) FHF-, (*E*) SHF-, and (*F*) nodal-like CMs ($n = 3$ biological replicates, three technical replicates each) (left) and isolated human foetal left and right ventricles (LV and RV, respectively) (right) ($n = 1$ biological replicates, three technical replicates each) for FHF (*TBX5* and *HAND1*), SHF (*ISL1 and TBX1*), and nodal genes *SHOX2, HCN4*, and *TBX18*. Immunocytochemistry analysis of Day 10 sorted (*G*) FHF- and (*H*) SHF-like, and (*I*) nodal-like cardiomyocytes for specific markers of FHF (TBX5), SHF (ISL1), and nodal cells (SHOX2). Presence of cardiomyocytes is indicated by expression of TNNT2 and all nuclei were visualized with DAPI. Scale bars = 20 µm. Statistical analysis is performed by using one-way ANOVA and Student's *t*-test, *$P < 0.05$, ** $P < 0.01$, *** $P < 0.001$, **** $P < 0.0001$. Error bar = SEM.

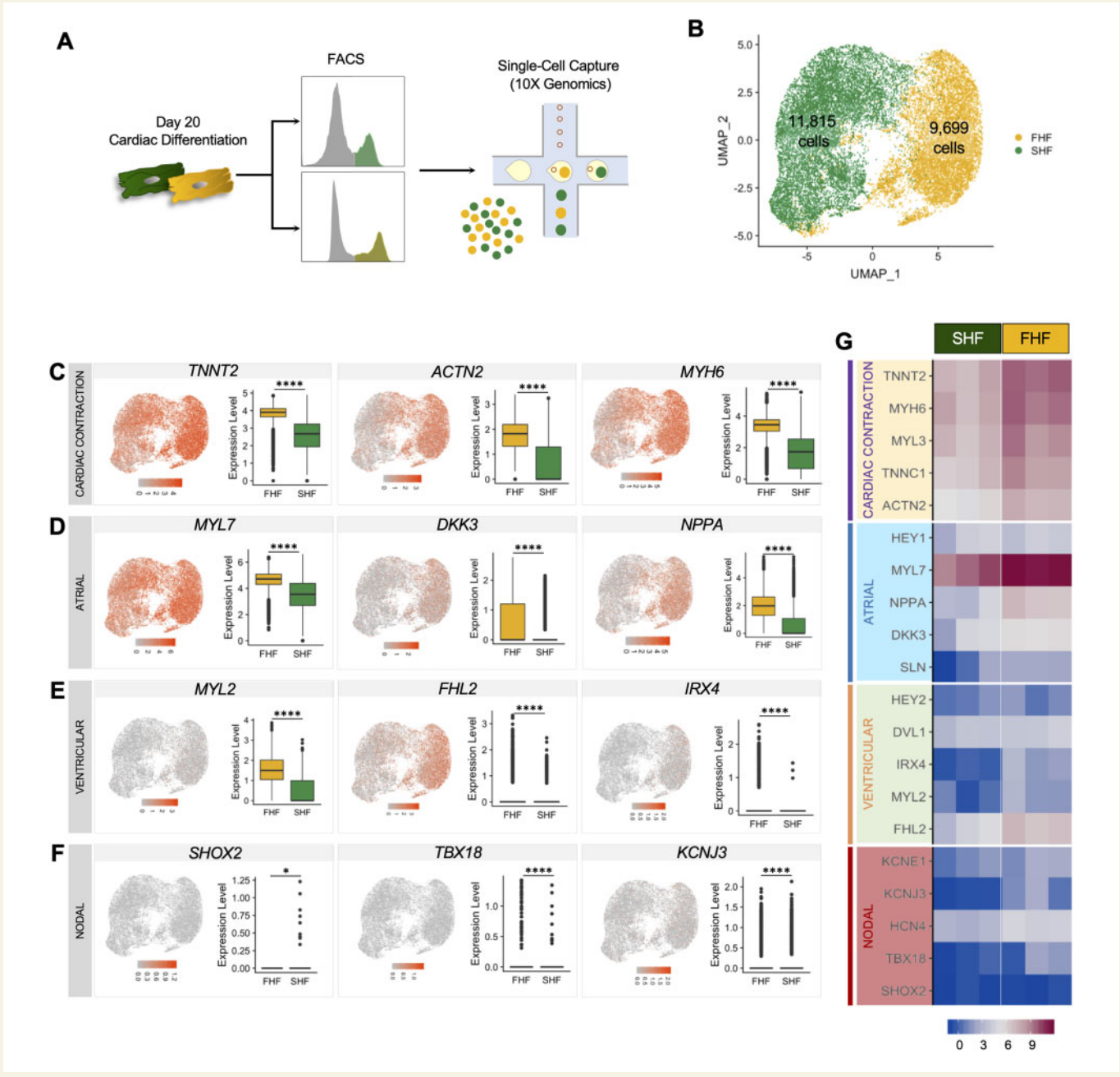

Figure 4 Single-cell RNA sequencing of FHF- and SHF-like cardiomyocytes. (*A*) Schematic of single cell capture using 10X Genomics. (*B*) UMAP showing cells labelled according to their input identity (FHF-like CMs: yellow, SHF-like CMs: green) (pool of three biological replicates, statistical analysis is performed by using Student's *t*-test, $*P < 0.05$, **** $P < 0.0001$.). UMAP and boxplots showing gene expression quantification for the (C) cardiac contractile genes *TNNT2*, *ACTN2*, and *MYH6*, (*D*) atrial genes *MYL7*, *DKK3*, and *NPPA*, (*E*) ventricular genes *MYL2*, *FHL2*, and *IRX4*, and (*F*) nodal genes *SHOX2*, *TBX18*, and *KCNJ3*. (*G*) Heatmaps from bulk RNA sequencing of Day 20 FHF and SHF populations showing genes corresponding to (*C–F*) ($n = 3$ biological replicates per group).

(*Figure 5C and D*). These electrophysiological results differ from those previously reported in hiPSCs.[39]

To further analyse the AP amplitude (APA) and maximum diastolic potential (MDP) of FHF and SHF-like CMs, we performed single-cell patch clamping, which reveal that both FHF and SHF populations had typical atrial and to lesser extent ventricular APs with fast upstroke velocities (> 30 V/s) and MDP (-60 ± 0.7 mV) (Supplementary material online, *Figure S4B*). Additionally, APA analysis shows no significant difference between FHF and SHF (combined average AP parameters from patch clamping and optical mapping are summarized in *Figure 5D*). To ensure that this difference in AP parameters is not due to more abundant ventricular APs in the FHF population, 78 atrial-like cells were selected from each population (AP with triangulation, no plateau) (Supplementary material online, *Figure S4C*). Binned histograms of atrial APD_{90} from each population show significantly longer APD_{90} in FHF compared to SHF (Supplementary material online, *Figure S4D*).

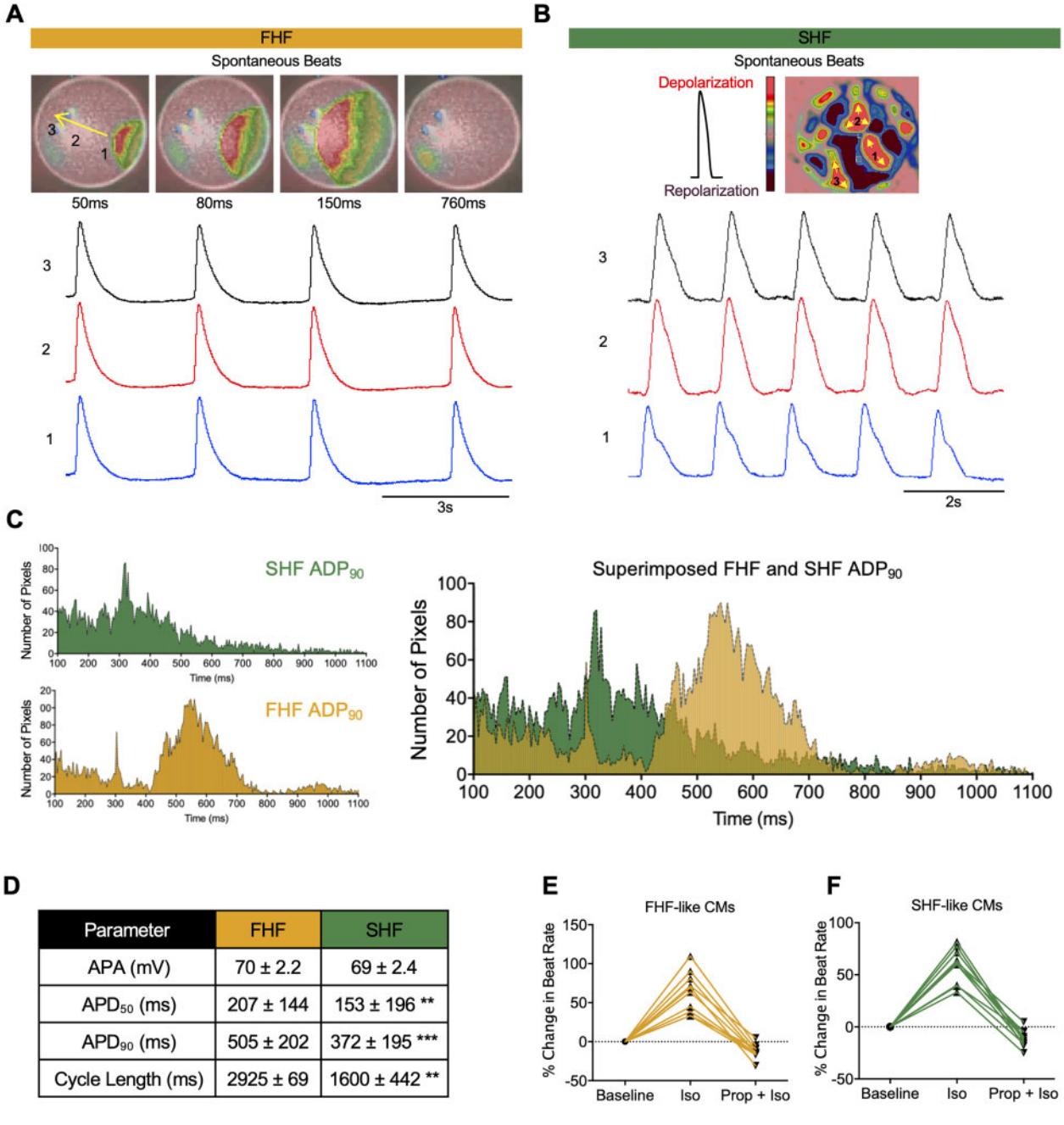

Parameter	FHF	SHF
APA (mV)	70 ± 2.2	69 ± 2.4
APD_{50} (ms)	207 ± 144	153 ± 196 **
APD_{90} (ms)	505 ± 202	372 ± 195 ***
Cycle Length (ms)	2925 ± 69	1600 ± 442 **

Figure 5 Electrophysiological analyses of FHF- and SHF-like cardiomyocytes. Snapshots of optical mapping show spontaneous AP which propagates across monolayer of (*A*) FHF-like CMs and (*B*) islands of SHF-like CMs (pool of three biological replicates). The yellow arrow denotes direction of AP propagation. Numbers denote the area where APs were recorded. Red and pink represent depolarized and repolarized phases, respectively. (*C*) APD_{90} histogram of APs recorded from FHF- (n = 6,660 pixels) and SHF-like CMs (n = 4,750 pixels). These histograms are superimposed on the right. (*D*) AP parameters of FHF- and SHF-like CMs (values are mean ± SD, statistical analysis is performed by using Student's t-test, ** P<0.01, *** P<0.001. APA was calculated from patch-clamp studies; all others were calculated from optical mapping experiments). Each pixel size = 10 x 10 μm. Beating rates of (*E*) FHF- and (*F*) SHF-like cardiomyocytes following application of β–adrenergic agonist (isoproterenol, Iso, 1 μM) and antagonist (propranolol, Prop, 10 μM) (n = 10 biological replicates).

We next examined the chronotropic responses of FHF- and SHF-like CMs to β-adrenergic drugs *in vitro*. Isoproterenol (1 μM), a β-adrenoreceptor agonist, enhance the contraction rates of both FHF- and SHF-like CMs, whereas addition of Propranolol (Prop) (10 μM), a β-adrenoreceptor antagonist result in recovery to the baseline contraction rate (*Figure 5E and F*, Supplementary material online, *Videos S5* and *S6*).

Lastly, we performed optical mapping analysis on TBX5+NKX2-5- population which shows characteristic nodal-like AP in which slow

depolarization (Phase 4), rapid depolarization (Phase 0), and repolarization (phase 3) are present (Supplementary material online, *Figure S4E*). APD distribution and parameters of 1,100 pixels were measured and summarized in Supplementary material online, *Figure S4F*. Immunocytochemistry of TBX5, ISL1, and SHOX2 with co-staining of TNNT2 shows expression of TBX5 and SHOX2 within this population but not ISL1 (Supplementary material online, *Figure S4G*).

Together, results from electrophysiological studies reflect the dominancy of atrial-like action potentials, coordination of channel activities, presence of functional gap junctions, and the ability to respond to pharmacological agents in hESC-derived CMs.

3.7 POPDC2 and CORIN are potential surface markers for the isolation of cardiomyocytes

Due to the lack of a robust method to isolate viable hESC-derived CMs without the use of a genetically modified reporter line, we sought to identify surface markers that are distinctly expressed on CPCs and continue to be expressed after differentiation into CMs utilizing our RNA sequencing dataset. We first identified differential gene expression of each cell population compared to hESC and combined those genes for input into the PANTHER Classification System. GO analysis of cellular component identifies 20 genes localized to the plasma membrane. Heatmap analysis reveals expression of these potential surface markers in differentiated cells across different time points, but not in hESC (*Figure 6A*). First, to confirm the specificity of these genes to the heart, we examined their expression in the Kaessman database.[47] Out of the 20 genes, four of them are highly expressed in the heart compared to other organs. Despite their specificity to the heart, it is possible that they may also be expressed on other cardiac-related cells such as vascular or mesenchymal cells in addition to CMs. To filter out candidates that may be expressed on other cardiac cell types, we first performed scRNA seq analysis of a human foetal heart (10 weeks of gestation). We identified endothelial, fibroblast, and CM cell populations based on established cell type markers (Supplementary material online, *Figure S5A*). Using these data, we discover *POPDC2* and *CORIN* from our candidate list to be the most specific to CMs in the human foetal heart. Heart field specificity analysis of these two candidates reveals *CORIN* as FHF-specific in hESC-derived CMs, whereas *POPDC2* is diffusely expressed in both FHF- and SHF-like CMs (*Figure 6B* and Supplementary material online, *Figure S5B*). qPCR analysis of *CORIN* shows its specificity in our FHF population as well as human LV (18-week gestation) (*Figure 6C*).

To determine whether CORIN can be used as a surface marker to isolate heart field-specific CMs, we first analysed CORIN$^+$ cells and found 90% are TNNT2-positive via flow cytometry (*Figure 6D*). We next performed flow cytometry analysis for CORIN$^+$ and CORIN$^-$ cells at Day 10. We observe that 73% of the CORIN$^+$ and only 14% of the CORIN$^-$ populations are FHF-like CMs (TBX5$^+$NKX2-5$^+$) if the differentiation is biased towards FHF-like CMs (*Figure 6E*, top). Interestingly, when the differentiation is biased towards SHF-like CMs, there are no CORIN$^+$ cells present in the SHF population (*Figure 6E*, bottom). As expected, isolated cells show higher expression of *TBX5* in CORIN$^+$ and *ISL1* in CORIN$^-$ populations (*Figure 6F*). ICC analysis also demonstrates that CORIN$^+$ cells exhibit high expression of TBX5, but low expression of ISL1 and SHOX2 suggesting that these cells display FHF-like CM phenotype (*Figure 6G*). We also performed optical mapping to assess the EP properties of CORIN$^+$ cells. AP propagation was recorded from spontaneous beating cells in CORIN$^+$ CMs. Optical mapping demonstrates that CORIN$^+$ cells have similar EP characteristics as the FHF-like CMs isolated from the double reporter hESC line (*Figure 6H* and Supplementary material online, *Video S7*). We observe diffuse but selective CORIN staining of CMs in the intact adult human LV (*Supplementary Figure 5C* and *D*). Finally, assessment of cell cycle activity between CORIN+ cells and undifferentiated hESC (D0) shows the expected decline in expression of cell cycle activators and increase in cell cycle inhibitors within CORIN+ cells.

To examine the versatility of CORIN to select for FHF-like cells from different cell lines, we first analysed *CORIN* expression in publicly available RNA sequencing databases (Supplementary material online, *Figure S6A* and *B*). We examined the expression of *CORIN* in hiPSC-derived cardiac cells (CMs, endothelial cells, fibroblasts, and epicardial cells) which show *CORIN* expression is confined to CMs (Supplementary material online, *Figure S6A*, GSE116464). To examine whether *CORIN* is selectively expressed in FHF CMs derived from hiPSCs, we used GSE102202 dataset in which they sequenced hiPSC-derived FHF, SHF, and nodal CMs. Consistent with findings from our double reporter, *CORIN* expression is limited to the FHF CMs (Supplementary material online, *Figure S6B*). Finally, to test whether CORIN selects for FHF cells in a different hESC cell line, H9 hESCs were differentiated, stained, and sorted for CORIN+ cells, which show 46% positivity compared to control (Supplementary material online, *Figure S6C*). ICC shows presence of cardiac contraction markers (TNNT2, ACTN2) and FHF marker (TBX5) within these cells (Supplementary material online, *Figure S6D*). These results support the notion that CORIN expression is maintained in CMs throughout cardiac differentiation and its utility in isolating FHF CMs from different hiPSC and hESC cell lines.

4. Discussion

Here, we report isolation and characterization of heart field-specific CMs from differentiating hESCs. Using a *TBX5*$^{TdTomato+/W}$/*NKX2-5*$^{eGFP/W}$ hESC double reporter line, we were able to generate three distinct populations that corresponded to the FHF-CMs, SHF-CMs, and nodal-like CMs. The ability to isolate pure population of these CM subtypes can facilitate a more rigorous approach for developmental studies, disease modelling, and drug screening as well as improving the clinical application of cardiac regenerative therapy. Current strategies to generate CMs from differentiating hESCs are limited in their ability to separate heart field-specific CMs and exclude contaminating nodal cells. This technical challenge has limited studies on the biological relevance of chamber-specific CMs and its potential role for more efficient regenerative therapies using hESC. Our studies reveal that TBX5 is sufficient to delineate between the first and second heart fields whereas the addition of NKX2-5 is necessary for the exclusion of pacemaker cells. We also discovered two novel surface markers, POPDC2 that allows isolation of CMs and CORIN that facilitates separation of FHF-CMs from other CM subtypes, without the use of a genetically modified cell line.

Following a typical MI, there is extensive loss of CMs, primarily localized to the LV of the heart. Although the adult heart consists of CMs from distinct embryonic origins that later localize to specific anatomical regions, it is not known whether their ontogeny influences their physiological function.[48–50] While some reports have shown similarities between LV and RV CMs, there are still observed differences with respect to their ion channels, structural proteins, and electrical properties.[51] There is considerable controversy on whether the observed differences can be attributed only to altered circulatory pressures during foetal

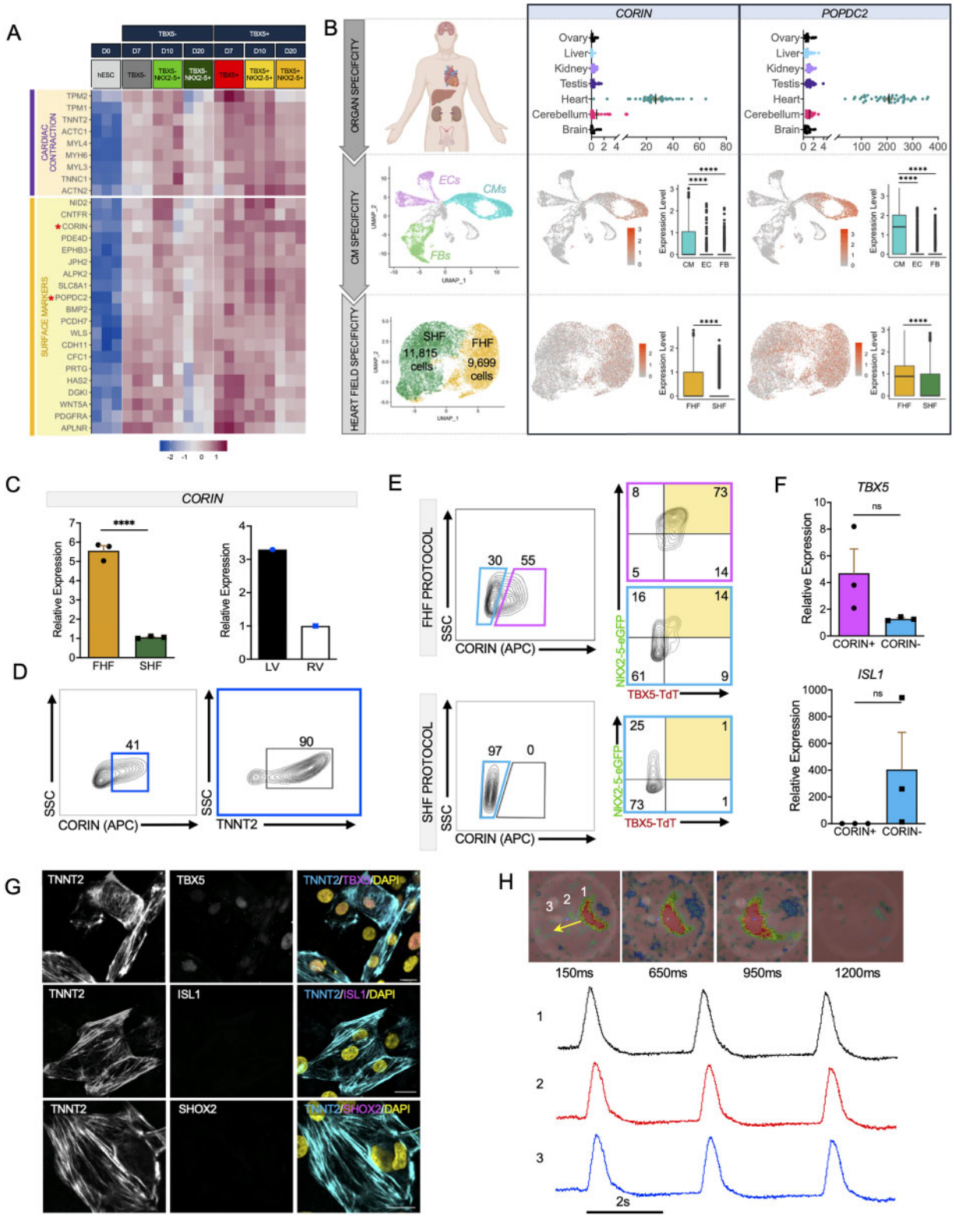

Figure 6 Isolation and enrichment of FHF-like CMs using the surface marker CORIN. (*A*) Heatmap showing co-expression of cardiac contraction and surface marker genes in TBX5^{+} and TBX5^{-} populations at different time points (three biological replicates per group). (*B*) *CORIN* and *POPDC2* expression assessed using the (top) Kaessmann online database[47] (one-way ANOVA, *P*-value (heart vs. other tissues, <0.0001), biological replicates: brain ($n = 52$), cerebellum ($n = 58$), heart ($n = 44$), kidney ($n = 36$), liver ($n = 49$), ovary ($n = 18$), testis ($n = 39$) for organ specificity, (middle) single-cell RNA sequencing analysis of human foetal heart (10-week gestation) for CM specificity (one biological replicate), and (bottom) Day 20 FHF- and SHF-like CMs for heart field specificity (pool of three biological replicates). (*C*) qPCR analysis of CORIN expression in (left) FHF and SHF-like CMs (three biological replicates, three technical replicates each) and (right) human foetal LV and RV (18-week gestation, one biological replicate, three technical replicates each). (*D*) Flow cytometric analysis of CORIN^{+} cells for TNNT2 expression (pool of 3 biological replicates). (*E*) Flow cytometric analysis of TBX5 and NKX2-5 in CORIN^{+} and CORIN^{-} cells

Figure 6 Continued
(pool of three biological replicates) using FHF (top) and SHF (bottom) protocols. (*F*) Quantitative PCR analysis of FHF (*TBX5*) and SHF (*ISL1*) in CORIN$^+$ and CORIN$^-$ Day 10 sorted cells (three biological replicates, three technical replicates each). (*G*) Immunocytochemistry of Day 10 sorted CORIN$^+$ CMs for markers of FHF (TBX5), SHF (ISL1), and nodal cells (SHOX2). Cardiomyocytes are shown by TNNT2 staining and all nuclei were shown by DAPI. Scale bar = 20 μm. (*H*) Snapshots of optical mapping show spontaneous AP propagation across monolayer of CORIN$^+$ CMs. The yellow arrow denotes direction of AP propagation. Numbers denote the area from which the APs were recorded. Red and pink represent depolarized and repolarized phases, respectively (pool of three biological replicates). Statistical analysis is performed by using Student's *t*-test, *$P < 0.05$, **** $P < 0.0001$, ns = not significant. Error bar = SEM.

development and after birth.[52,53] However, this explanation contradicts observations of RV failure in congenital heart defects in which the RV acts as a systemic ventricle. This suggests that there may be inherent differences between LV and RV CMs beyond their exposure to different pressure loads. From a cardiac regeneration perspective, no study has yet investigated whether transplantation of chamber-specific CMs can effectively compensate for the loss of cardiac function. We postulate that transplantation of LV CMs may enhance their engraftment, reduce the risk of arrhythmias, and improve cardiac function. However, no study has yet demonstrated the ability to purify LV CMs from hESCs for preclinical transplantation studies. To achieve this, it is imperative to be able to separate FHF from SHF CMs in addition to directing the CMs towards a ventricular phenotype.

In a recent study, Zhang et al. developed a hiPSCs double reporter using TBX5 and NKX2-5 in which they reported the isolation of FHF- and SHF-like CMs as well as endothelial and epicardial lineages. While this was a unique approach, there were some limitations, including the targeting strategy to generate their double reporter, low efficiency of heart field-directed cardiac differentiation, contamination of different cell types within each population, and small sample size in their EP studies. Questions remain regarding the specificity of TBX5 in delineating FHF cardiac cells. Our study addresses some of the former limitations and uncovers the early transcriptional profiles of cardiogenesis in hESCs. These findings can be used to better understand the complexity of transcriptional factor interactions in cardiac fate decisions *in vitro*.

Our bulk RNA sequencing results demonstrated that TBX5 expression is sufficient to distinguish FHF and SHF CPCs based on known heart field-specific markers. GO analysis showed that cardiac-related pathways were fairly enriched in TBX5$^+$ population at Day 7; however, TBX5$^-$ population was enriched with more non-CM related pathways. Interestingly, the expression of nodal-related markers was highly enriched in TBX5$^+$ population in which the ISL1 expression was significantly low. This finding is different from the previous study in which the expression of both TBX5 and ISL1 was high.[39] The addition of NKX2-5 as a pan-CPC marker was necessary to further purify CMs from nodal and other non-CMs within these two heart field populations. When we compared TBX5$^-$/NKX2-5$^+$ populations (Days 10 and 20) with TBX5$^-$ population (Day 7), we found a shift of the GO terms towards CM related pathways. We also observed expression of atrial and ventricular but not nodal genes in both heart fields, with higher expression within FHF populations. Further analysis of atrial and ventricular markers using our scRNA seq data showed that more cells in both populations express atrial-related genes rather than ventricular. Even after prolonged culture to allow cells to become more mature (Day 20 of differentiation), we observed a dominance of atrial related genes in both single cell and bulk RNA sequencing.

To investigate potential differences in EP properties and assess their ability to form a functional syncytium, we performed single-cell patch clamping and optical mapping studies on the isolated FHF-, SHF-, and nodal-like CMs. Consistent with our gene expression data, we found that FHF- and SHF-like CMs are predominantly composed of atrial and, to a lesser extent, ventricular CMs. They displayed similar electrical wavefront activation establishing electrical coupling and regenerative AP propagation during spontaneous depolarization. The relatively rapid rise in action potential (dV/dtmax) in patch-clamp studies suggested the presence of voltage-activated channels (Na^+ channels) in both FHF and SHF CMs. In order to determine whether a cell is atrial or ventricular from an EP standpoint, two important criteria must be considered: morphology and duration of AP. Morphology of ventricular AP is defined by a prominent plateau phase which is largely due to activation of L-type Ca^{2+} channel, whereas atrial APs are more triangularly shaped. Results from our optical mapping show that while FHF and SHF populations exhibited predominantly atrial AP morphology, there was a small percentage of ventricular-like APs (prominent plateau), which was higher in the FHF population compared to SHF. For analysis of AP duration, we performed optical mapping of almost 10,000 APDs in FHF and SHF CMs, which enabled us to gain a broader picture of AP duration in these two populations. These extensive analyses revealed significantly higher APD_{50}, APD_{90}, and cycle length in FHF population compared to SHF. Prolongation of average APs in FHF population could be due to 1) the presence of more ventricular morphologies which could be explained by higher expression of L-type Ca^{2+} channel (*CACNA1C*) observed in our scRNA seq (data not shown) or 2) inherent differences between FHF and SHF APs. Our results suggest the inherent differences between these two populations, as direct comparison of atrial APs (exclusion of APs that exhibit plateau), show significantly higher APD_{90} in FHF compared to SHF CMs. Our APD results differ from previously reported in hiPSC-derived FHF and SHF. These discrepancies could be due to intrinsic differences between hESC and iPSC cells, the technical knock-in strategies used to design these reporter lines, or inadequate sample for analysing APDs in FHF and SHF populations. Conduction velocities (CV) in FHF and SHF (in 2-dimensional fashion) were 0.11 m/s and 0.05 m/s, respectively, which is slower than reported in human CMs.[54] While several factors could account for these slower CVs (i.e. myocardial excitability and gap junction conductance and density), a major contributor could be the relatively positive resting diastolic membrane potential (observed in our patch-clamp data) which promotes sodium channel inactivation.[55] Our functional and molecular analyses provide robust evidence in the ability of our double reporter and differentiation strategies to isolate heart field specific CMs, which can provide an *in vitro* source for the generation of left- and right-ventricular like CMs. However, our protocols give rise to a predominantly atrial CM subtype. Given these observations, our study provides a platform by which chamber-specific (i.e. LV CMs) can be generated by modifying our FHF protocol to direct cells towards a ventricular phenotype, providing a highly desirable and specialized CM population for regenerative therapy.

For future therapeutic applications, it is important to be able to isolate FHF CMs without the use of a genetically modified hESC line. As such, we aimed to find novel surface markers that could be used as a potential surrogate of our double reporter. From our analysis of genes distinctly expressed on CPCs and their differentiated progeny, we identified 20 plasma membrane-associated genes. Of them, *CORIN* and *POPDC2* were found to be most specific to CMs in human foetal and adult hearts. Heart field specificity analysis of our and publicly available datasets revealed CORIN as FHF-specific in hESC- and hiPSC-derived CMs. CORIN is a serine protease in CMs responsible for the conversion of pro-atrial and pro-brain natriuretic peptides to their active forms and has been suggested as a biomarker in hypertension, cardiac hypertrophy, and heart failure.[56–60] Interestingly, CORIN is activated by the proprotein convertase subtilisin/kexin type 6 enzyme, encoded by *PCSK6*, a gene shown to be co-expressed with *TBX5* and involved in the development of left and right asymmetry.[61]

In summary, myocardial infarction leads to irreversible loss of cardiomyocytes and eventually heart failure. Despite the potential of hESCs as a source of cell therapy for cardiac regeneration, current differentiation strategies yield a mixture of cardiomyocyte subtypes and safety concerns stemming from the use of a heterogenous population of cardiomyocytes have hindered its application. Here, we describe a high-yield approach for isolation and characterization of hESC-derived FHF-, SHF-, and nodal-like CMs. Obtaining enriched populations of these different CM subtypes increases the resolution of gene expression profiling during early cardiogenesis, arrhythmia modelling, and drug screening. This also paves the way for the development of effective stem cell therapy to treat diseases that affect specific regions of the heart, such as MI involving the LV or chamber-specific congenital heart defects.

Supplementary material

Supplementary material is available at *Cardiovascular Research* online.

Acknowledgements

We would like to acknowledge H.S.K. and T.P.N. for the use of their electrophysiology instruments and consultation and the UCLA BSCRC FACS and Microscopy Cores. Human foetal heart samples were generously provided by the Translational Pathology Core Laboratory of the Department of Pathology and Laboratory Medicine at UCLA. The Corin antibody was a generous gift from Y.O. (KAN Research Institute, Japan), and the HES3 NKX2-5eGFP line was a kind gift from E.S. and A.E. (Monash University, Australia).

Conflict of interest: none declared.

Funding

This work was supported in part by grants from the Eli & Edythe Broad Center of Regenerative Medicine and Stem Cell Research at UCLA Postdoctoral Fellowship (A.P.), Department of Defense Discovery Award (PR182456) (A.P.), Ruth L. Kirschstein Predoctoral Fellowship (HL144057) (N.B.N), California Institute for Regenerative Medicine (CIRM) (RN3-06378) (R.A.), National Institute of Health R01HL148714 (R.A.), and UCLA BSCRC-Rose Hills Foundation Research Award (R.A.), and the Eli and Edythe Broad Foundation Innovative Pilot Stem Cell Research Grant (R.A.).

Data availability

The RNA sequencing data have been deposited in the GEO repository with GEO accession number GSE114373.

References

1. Arkell RM, Fossat N, Tam PP. Wnt signalling in mouse gastrulation and anterior development: new players in the pathway and signal output. *Curr Opin Genet Dev* 2013;**23**:454–460.
2. Cornell RA, Kimelman D. Activin-mediated mesoderm induction requires FGF. *Development* 1994;**120**:453–462.
3. Weinstein DC, Marden J, Carnevali F, Hemmati-Brivanlou A. FGF-mediated mesoderm induction involves the Src-family kinase Laloo. *Nature* 1998;**394**:904–908.
4. Winnier G, Blessing M, Labosky PA, Hogan BL. Bone morphogenetic protein-4 is required for mesoderm formation and patterning in the mouse. *Genes Dev* 1995;**9**:2105–2116.
5. Cheng P, Andersen P, Hassel D, Kaynak BL, Limphong P, Juergensen L, Kwon C, Srivastava D. Fibronectin mediates mesendodermal cell fate decisions. *Development* 2013;**140**:2587–2596.
6. Später D, Abramczuk MK, Buac K, Zangi L, Stachel MW, Clarke J, Sahara M, Ludwig A, Chien KR. A HCN4+ cardiomyogenic progenitor derived from the first heart field and human pluripotent stem cells. *Nat Cell Biol* 2013;**15**:1098–1106.
7. Bruneau BG, Logan M, Davis N, Levi T, Tabin CJ, Seidman JG, Seidman CE. Chamber-specific cardiac expression of Tbx5 and heart defects in Holt-Oram syndrome. *Dev Biol* 1999;**211**:100–108.
8. Watanabe Y, Zaffran S, Kuroiwa A, Higuchi H, Ogura T, Harvey RP, Kelly RG, Buckingham M. Fibroblast growth factor 10 gene regulation in the second heart field by Tbx1, Nkx2-5, and Islet1 reveals a genetic switch for down-regulation in the myocardium. *Proc Natl Acad Sci USA* 2012;**109**:18273–18280.
9. Zhou Z, Wang J, Guo C, Chang W, Zhuang J, Zhu P, Li X. Temporally Distinct Six2-Positive Second Heart Field Progenitors Regulate Mammalian Heart Development and Disease. *Cell Rep* 2017;**18**:1019–1032.
10. Francou A, Saint-Michel E, Mesbah K, Théveniau-Ruissy M, Rana MS, Christoffels VM, Kelly RG. Second heart field cardiac progenitor cells in the early mouse embryo. *Biochim Biophys Acta* 2013;**1833**:795–798.
11. Cai CL, Liang X, Shi Y, Chu PH, Pfaff SL, Chen J, Evans S. Isl1 identifies a cardiac progenitor population that proliferates prior to differentiation and contributes a majority of cells to the heart. *Dev Cell* 2003;**5**:877–889.
12. Lescroart F, Chabab S, Lin X, Rulands S, Paulissen C, Rodolosse A, Auer H, Achouri Y, Dubois C, Bondue A, Simons BD, Blanpain C. Early lineage restriction in temporally distinct populations of Mesp1 progenitors during mammalian heart development. *Nat Cell Biol* 2014;**16**:829–840.
13. Bu L, Jiang X, Martin-Puig S, Caron L, Zhu S, Shao Y, Roberts DJ, Huang PL, Domian IJ, Chien KR. Human ISL1 heart progenitors generate diverse multipotent cardiovascular cell lineages. *Nature* 2009;**460**:113–117.
14. Meilhac SM, Esner M, Kelly RG, Nicolas JF, Buckingham ME. The clonal origin of myocardial cells in different regions of the embryonic mouse heart. *Dev Cell* 2004;**6**:685–698.
15. Sun Y, Liang X, Najafi N, Cass M, Lin L, Cai CL, Chen J, Evans SM. Islet 1 is expressed in distinct cardiovascular lineages, including pacemaker and coronary vascular cells. *Dev Biol* 2007;**304**:286–296.
16. Ahlgren U, Pfaff SL, Jessell TM, Edlund T, Edlund H. Independent requirement for ISL1 in formation of pancreatic mesenchyme and islet cells. *Nature* 1997;**385**:257–260.
17. Ghazizadeh Z, Fattahi F, Mirzaei M, Bayersaikhan D, Lee J, Chae S, Hwang D, Byun K, Tabar MS, Taleahmad S, Mirshahvaladi S, Shabani P, Fonoudi H, Haynes PA, Baharvand H, Aghdami N, Evans T, Lee B, Salekdeh GH. Prospective Isolation of ISL1. *Stem Cell Rep* 2018;**10**:848–859.
18. Li QY, Newbury-Ecob RA, Terrett JA, Wilson DI, Curtis AR, Yi CH, Gebuhr T, Bullen PJ, Robson SC, Strachan T, Bonnet D, Lyonnet S, Young ID, Raeburn JA, Buckler AJ, Law DJ, Brook JD. Holt-Oram syndrome is caused by mutations in TBX5, a member of the Brachyury (T) gene family. *Nat Genet* 1997;**15**:21–29.
19. Liberatore CM, Searcy-Schrick RD, Yutzey KE. Ventricular expression of tbx5 inhibits normal heart chamber development. *Dev Biol* 2000;**223**:169–180.
20. Sizarov A, Devalla HD, Anderson RH, Passier R, Christoffels VM, Moorman AF. Molecular analysis of patterning of conduction tissues in the developing human heart. *Circ Arrhythm Electrophysiol* 2011;**4**:532–542.
21. Xie L, Hoffmann AD, Burnicka-Turek O, Friedland-Little JM, Zhang K, Moskowitz IP. Tbx5-hedgehog molecular networks are essential in the second heart field for atrial septation. *Dev Cell* 2012;**23**:280–291.
22. Devine WP, Wythe JD, George M, Koshiba-Takeuchi K, Bruneau BG. Early patterning and specification of cardiac progenitors in gastrulating mesoderm. *Elife* 2014;**3**:e03848.
23. Mummery CL, Zhang J, Ng ES, Elliott DA, Elefanty AG, Kamp TJ. Differentiation of human embryonic stem cells and induced pluripotent stem cells to cardiomyocytes: a methods overview. *Circ Res* 2012;**111**:344–358.
24. Murry CE, Keller G. Differentiation of embryonic stem cells to clinically relevant populations: lessons from embryonic development. *Cell* 2008;**132**:661–680.
25. Passier R, Denning C, Mummery C. Cardiomyocytes from human embryonic stem cells. *Handb Exp Pharmacol* 2006;101–122.

26. Den Hartogh SC, Schreurs C, Monshouwer-Kloots JJ, Davis RP, Elliott DA, Mummery CL, Passier R. Dual reporter MESP1 mCherry/w-NKX2-5 eGFP/w hESCs enable studying early human cardiac differentiation. *Stem Cells* 2015;**33**:56–67.
27. Elliott DA, Braam SR, Koutsis K, Ng ES, Jenny R, Lagerqvist EL, Biben C, Hatzistavrou T, Hirst CE, Yu QC, Skelton RJ, Ward-van Oostwaard D, Lim SM, Khammy O, Li X, Hawes SM, Davis RP, Goulburn AL, Passier R, Prall OW, Haynes JM, Pouton CW, Kaye DM, Mummery CL, Elefanty AG, Stanley EG. NKX2-5(eGFP/w) hESCs for isolation of human cardiac progenitors and cardiomyocytes. *Nat Methods* 2011;**8**:1037–1040.
28. Kitajima S, Miyagawa-Tomita S, Inoue T, Kanno J, Saga Y. Mesp1-nonexpressing cells contribute to the ventricular cardiac conduction system. *Dev Dyn* 2006;**235**:395–402.
29. Lints TJ, Parsons LM, Hartley L, Lyons I, Harvey RP. Nkx-2.5: a novel murine homeobox gene expressed in early heart progenitor cells and their myogenic descendants. *Development* 1993;**119**:969.
30. Lyons I, Parsons LM, Hartley L, Li R, Andrews JE, Robb L, Harvey RP. Myogenic and morphogenetic defects in the heart tubes of murine embryos lacking the homeo box gene Nkx2-5. *Genes Dev* 1995;**9**:1654–1666.
31. Prall OW, Menon MK, Solloway MJ, Watanabe Y, Zaffran S, Bajolle F, Biben C, McBride JJ, Robertson BR, Chaulet H, Stennard FA, Wise N, Schaft D, Wolstein O, Furtado MB, Shiratori H, Chien KR, Hamada H, Black BL, Saga Y, Robertson EJ, Buckingham ME, Harvey RP. An Nkx2-5/Bmp2/Smad1 negative feedback loop controls heart progenitor specification and proliferation. *Cell* 2007;**128**:947–959.
32. Saga Y, Kitajima S, Miyagawa-Tomita S. Mesp1 expression is the earliest sign of cardiovascular development. *Trends Cardiovasc Med* 2000;**10**:345–352.
33. Chong JJ, Yang X, Don CW, Minami E, Liu YW, Weyers JJ, Mahoney WM, Van Biber B, Cook SM, Palpant NJ, Gantz JA, Fugate JA, Muskheli V, Gough GM, Vogel KW, Astley CA, Hotchkiss CE, Baldessari A, Pabon L, Reinecke H, Gill EA, Nelson V, Kiem HP, Laflamme MA, Murry CE. Human embryonic-stem-cell-derived cardiomyocytes regenerate non-human primate hearts. *Nature* 2014;**510**:273–277.
34. Laflamme MA, Chen KY, Naumova AV, Muskheli V, Fugate JA, Dupras SK, Reinecke H, Xu C, Hassanipour M, Police S, O'Sullivan C, Collins L, Chen Y, Minami E, Gill EA, Ueno S, Yuan C, Gold J, Murry CE. Cardiomyocytes derived from human embryonic stem cells in pro-survival factors enhance function of infarcted rat hearts. *Nat Biotechnol* 2007;**25**:1015–1024.
35. Shiba Y, Gomibuchi T, Seto T, Wada Y, Ichimura H, Tanaka Y, Ogasawara T, Okada K, Shiba N, Sakamoto K, Ido D, Shiina T, Ohkura M, Nakai J, Uno N, Kazuki Y, Oshimura M, Minami I, Ikeda U. Allogeneic transplantation of iPS cell-derived cardiomyocytes regenerates primate hearts. *Nature* 2016;**538**:388–391.
36. Park S, Nguyen NB, Pezhouman A, Ardehali R. Cardiac fibrosis: potential therapeutic targets. *Transl Res* 2019;**209**:121–137.
37. Hiroi Y, Kudoh S, Monzen K, Ikeda Y, Yazaki Y, Nagai R, Komuro I. Tbx5 associates with Nkx2-5 and synergistically promotes cardiomyocyte differentiation. *Nat Genet* 2001;**28**:276–280.
38. Protze SI, Liu J, Nussinovitch U, Ohana L, Backx PH, Gepstein L, Keller GM. Sinoatrial node cardiomyocytes derived from human pluripotent cells function as a biological pacemaker. *Nat Biotechnol* 2017;**35**:56–68.
39. Zhang JZ, Termglinchan V, Shao NY, Itzhaki I, Liu C, Ma N, Tian L, Wang VY, Chang ACY, Guo H, Kitani T, Wu H, Lam CK, Kodo K, Sayed N, Blau HM, Wu JC. A human iPSC double-reporter system enables purification of cardiac lineage subpopulations with distinct function and drug response profiles. *Cell Stem Cell* 2019;**24**:802–811.
40. Lian X, Zhang J, Azarin SM, Zhu K, Hazeltine LB, Bao X, Hsiao C, Kamp TJ, Palecek SP. Directed cardiomyocyte differentiation from human pluripotent stem cells by modulating Wnt/β-catenin signaling under fully defined conditions. *Nat Protoc* 2013;**8**:162–175.
41. Wu J, Anczuków O, Krainer AR, Zhang MQ, Zhang C. OLego: fast and sensitive mapping of spliced mRNA-Seq reads using small seeds. *Nucleic Acids Res* 2013;**41**:5149–5163.
42. Liao Y, Smyth GK, Shi W. featureCounts: an efficient general purpose program for assigning sequence reads to genomic features. *Bioinformatics* 2014;**30**:923–930.
43. Birket MJ, Ribeiro MC, Verkerk AO, Ward D, Leitoguinho AR, den Hartogh SC, Orlova VV, Devalla HD, Schwach V, Bellin M, Passier R, Mummery CL. Expansion and patterning of cardiovascular progenitors derived from human pluripotent stem cells. *Nat Biotechnol* 2015;**33**:970–979.
44. Pezhouman A, Cao H, Fishbein MC, Belardinelli L, Weiss JN, Karagueuzian HS. Atrial fibrillation initiated by early afterdepolarization-mediated triggered activity during acute oxidative stress: efficacy of late sodium current blockade. *J Heart Health* 2018;**4**. doi:10.16966/2379-769X.146.
45. Pezhouman A, Singh N, Song Z, Nivala M, Eskandari A, Cao H, Bapat A, Ko CY, Nguyen T, Qu Z, Karagueuzian HS, Weiss JN. Molecular basis of hypokalemia-induced ventricular fibrillation. *Circulation* 2015;**132**:1528–1537.
46. Pezhouman A, Madahian S, Stepanyan H, Ghukasyan H, Qu Z, Belardinelli L, Karagueuzian HS. Selective inhibition of late sodium current suppresses ventricular tachycardia and fibrillation in intact rat hearts. *Heart Rhythm Off J Heart Rhythm Soc* 2014;**11**:492–501.
47. Cardoso-Moreira M, Halbert J, Valloton D, Velten B, Chen C, Shao Y, Liechti A, Ascenção K, Rummel C, Ovchinnikova S, Mazin PV, Xenarios I, Harshman K, Mort M, Cooper DN, Sandi C, Soares MJ, Ferreira PG, Afonso S, Carneiro M, Turner JMA, VandeBerg JL, Fallahshahroudi A, Jensen P, Behr R, Lisgo S, Lindsay S, Khaitovich P, Huber W, Baker J, Anders S, Zhang YE, Kaessmann H. Gene expression across mammalian organ development. *Nature* 2019;**571**:505–509.
48. Kelly RG. The second heart field. *Curr Top Dev Biol* 2012;**100**:33–65.
49. Zaffran S, Kelly RG. New developments in the second heart field. *Differentiation* 2012;**84**:17–24.
50. Dyer LA, Kirby ML. The role of secondary heart field in cardiac development. *Dev Biol* 2009;**336**:137–144.
51. Zhao X-S, Gallardo TD, Lin L, Schageman JJ, Shohet RV. Transcriptional mapping and genomic analysis of the cardiac atria and ventricles. *Physiol Genomics* 2002;**12**:53–60.
52. Molina CE, Heijman J, Dobrev D. Differences in left versus right ventricular electrophysiological properties in cardiac dysfunction and arrhythmogenesis. *Arrhythm Electrophysiol Rev* 2016;**5**:14–19.
53. Kondo RP, Dederko DA, Teutsch C, Chrast J, Catalucci D, Chien KR, Giles WR. Comparison of contraction and calcium handling between right and left ventricular myocytes from adult mouse heart: a role for repolarization waveform. *J Physiol* 2006;**571**:131–146.
54. Harrild D, Henriquez C. A computer model of normal conduction in the human atria. *Circ Res* 2000;**87**:E25–E36.
55. Liu J, Laksman Z, Backx PH. The electrophysiological development of cardiomyocytes. *Adv Drug Deliv Rev* 2016;**96**:253–273.
56. Zhou X, Chen JC, Liu Y, Yang H, Du K, Kong Y, Xu XH. Plasma corin as a predictor of cardiovascular events in patients with chronic heart failure. *JACC Heart Fail* 2016;**4**:664–669.
57. Feistritzer HJ, Klug G, Reinstadler SJ, Reindl M, Mayr A, Mair J, Metzler B. Novel biomarkers predicting cardiac function after acute myocardial infarction. *Br Med Bull* 2016;**119**:63–74.
58. Yan W, Wu F, Morser J, Wu Q. Corin, a transmembrane cardiac serine protease, acts as a pro-atrial natriuretic peptide-converting enzyme. *Proc Natl Acad Sci USA* 2000;**97**:8525–8529.
59. Wu Q. The serine protease corin in cardiovascular biology and disease. *Front Biosci* 2007;**12**:4179–4190.
60. Zhou Y, Wu Q. Corin in natriuretic peptide processing and hypertension. *Curr Hypertens Rep* 2014;**16**:415.
61. Constam DB, Robertson EJ. SPC4/PACE4 regulates a TGFbeta signaling network during axis formation. *Genes Dev* 2000;**14**:1146–1155.

Translational perspective

Myocardial infarction leads to irreversible loss of cardiomyocytes and eventually heart failure. Human embryonic stem cells (hESCs) can be differentiated to cardiomyocytes and are considered a potential source of cell therapy for cardiac regeneration. However, current differentiation strategies yield a mixture of cardiomyocyte subtypes, and safety concerns stemming from the use of a heterogenous population of cardiomyocytes have hindered its application. Here, we report generation of enriched heart field-specific cardiomyocytes using a hESC double reporter. Our study facilitates investigating early human cardiogenesis *in vitro* and generating chamber-specific cardiomyocytes to treat diseases that affect specific regions of the heart.